On the influence of secondary branches on crack propagation in Rolling Contact Fatigue

Mael Zaid, V. Doquet, Vincent Chiaruttini, Pierre Depouhon, Vincent Bonnand, Didier Pacou

On the influence of secondary branches on crack propagation in Rolling Contact Fatigue

Mael Zaid[1], Véronique Doquet[3], Vincent Chiaruttini[2], Pierre Depouhon[1], Vincent Bonnand[2], Didier Pacou[2]

[1]*Airbus Helicopters, Aéroport International Marseille Provence, 13700 Marignane*

[2]*Université Paris-Saclay, ONERA, Matériaux et Structures, 92322, Châtillon, France*

[3]*Laboratoire de Mécanique des Solides, CNRS, UMR 7649, Ecole Polytechnique, Institut Polytechnique de Paris, France*

Corresponding author: mael.zaid@airbus.com

Abstract: Gear and bearing failures are most often caused by rolling contact fatigue (RCF). Understanding the growth of a main surface-initiated crack into the depth of the piece, as well as the growth of subsurface-initiated branches towards the surface is necessary, in order to improve fatigue life prediction and reduce fatigue damage repair or component replacements before catastrophic failure. The purpose of this work is to analyze, based on 3D finite element simulations, the initiation and mode I growth of secondary branches in a case hardened gear, their influence on the main crack growth in mode II, and the competition between mode I and mode II crack growth. The residual stress field issued by the case hardening is taken into account and its role is analyzed. The reasons why branch cracks develop only from the upper main crack face and why only those initiated when the main crack is still shallow can reach the surface, inducing spalling are explained.

Keywords: Rolling contact fatigue, Branch crack, Spalling, Compression, Fatigue crack, Residual stress, Crack path

Introduction

Subsurface crack growth in rolling contact fatigue (RCF) is a common phenomenon in gears, bearing and rails [1-4]. These cracks can initiate from surface-originated pitting [5-7], or subsurface-initiated spalling [8]. A better understanding of the fatigue process is necessary to improve fatigue life prediction, and reduce fatigue damage to repair, or to replace components before a catastrophic failure.

One of the difficulties encountered in that task comes from the case hardening, often applied on these components, inducing a gradient in microstructure and mechanical properties, as well as residual stresses.

In RCF, according to Rycerz and al. [9], the crack path has many points where the propagation direction changes locally, forming nearly 90° zig-zags. Such "steps" are often associated with mode II loading. Suresh [10] points out that this type of morphology significantly reduces the effective driving force for shear propagation, due to interlocking and friction between the asperities.

Many authors working on RCF in bearings, [9, 11, 12] but also in rails [11, 13] noted the presence, along the flanks of the main crack growing in mode II, of many secondary cracks initially inclined by 75° to 80° relative to the main crack growth direction (Figure 1a), that grow towards the surface, inducing spalling of the contact surface, characterized by the release of fragment of the material (metal particles) in the lubricated environment. In case-hardened gears, these secondary branches develop from 0 to 0.3 mm depth, only from the upper flank of the main crack (Figure 1b), while in laboratory tests on cracked samples loaded in reversed mode II with a static uniaxial [14, 15], or biaxial [16] compression superimposed, such secondary cracks are distributed equally on both crack lips.

Figure 1a also shows that in the illustrated case, the branches initiated when the main crack was less than 0.35 mm deep reached the surface, inducing spalls, while those initiated later, (labelled

1 to 20 on figure 1a) did not reach the surface.

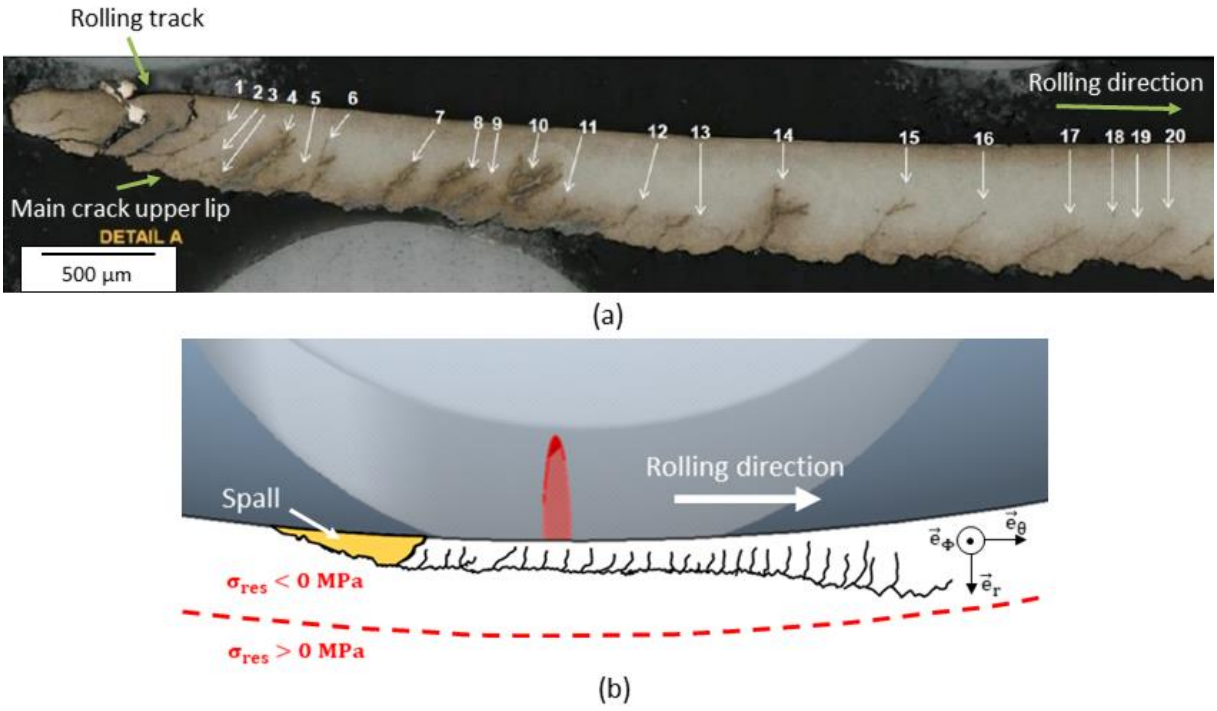

Figure 1 : (a) Propagation of secondary branches along the main crack upper lip in an helicopter gear subjected to rolling contact fatigue (observations made by Airbus Helicopters), (b) Typical subsurface propagation of a crack in a case-hardened helicopter gear submitted to RCF

Once initiated, these branches are mainly loaded in cyclic mode I at R = -1 [17, 18], with a ΔK_I that increases with ΔK_{II} at the tip of the main crack, and decreases with their distance from this tip. This may allow them to grow, reach the surface, and generate spalls, or, if the main crack propagates fast enough, reducing ΔK_I at the branch crack tip, to stop growing, if ΔK_I drops below the threshold. To monitor the damage of the parts in the gear boxes, magnetic plugs collect the particles generated by spalling, until a certain accumulation indicates the need to change the bearings. However, the reliability of this monitoring depends on the ability of the branches to reach the surface.

The influence of such branches on a crack loaded in shear mode has been analyzed [16-18]. Doquet and Frelat [18] highlighted the shielding effect exerted by the branches, which reduces

the driving force of the main crack. This effect was shown to increase with the number of branches [16]. Thus, once these branches initiate, a competition is observed between the main crack -loaded in mode II- and the branches -loaded in mode I [16, 18]. The issue of this competition in an helicopter gear (spalling or not, which is of primary importance for the reliability of damage monitoring by debris collection in the lubricant) depends on the compressive stress field induced by rolling contact loading plus the residual stress field left by case hardening. Zaid and al. [16] analyzed numerically in 2D for a center crack in a large plate, the influence of a static compressive stress T_x parallel to the main crack, or a static compressive stress T_y normal to the main crack, or the combination of both these stresses on the competition between a main crack loaded in reversed mode II and a quasi-normal branch located some distance behind its tip, loaded in mode I. They noted that an increase of the compressive T_x stress reduces ΔK_I of the branch, and thus its shielding effect on the main crack, so that $\Delta K_{II,eff}$ of the main crack slightly increases. They concluded that a negative T_x stress inhibits secondary branch crack growth, and promotes mode II propagation, as experimentally observed by Otsuka and al. [15] and Nishizawa and Ogawa [19]. Normal compression T_y was found to reduces $\Delta K_{II,eff}$, but even more ΔK_I for the branch crack, also favoring mode II propagation of the main crack.

The fatigue damage of a case-hardened gear and the ability to detect this damage are controlled by the competition between a main crack and secondary branches. It is thus of prime importance to analyze it in a more realistic way.

The purpose of this paper is thus to analyze the initiation and growth of secondary branches in an industrial component, and their influence on the main crack (figure 1b). To this end, a 3D finite element model taking into account the residual stress field, induced by case hardening, was developed, and the stress intensity factors (SIFs) for the main crack and branches were

computed. The link between spalling and subsurface crack was highlighted through the study of secondary branches. The end of the spalling phenomenon beyond a certain main crack depth is explained by the arrest of secondary branches.

NUMERICAL MODEL

In the context of a case-hardened gear, the propagation of a crack occurs within a complex environment influenced by various phenomena. These include residual stresses, variations in mechanical properties, Hertzian loading, and structural effects. Attempting to capture all these aspects accurately can pose a challenge for 2D numerical or simplified analytical models. Therefore, to ensure a comprehensive representation of the gear in service, a 3D finite element model has been developed. This approach enables the consideration of all relevant factors, and provides a more realistic understanding of crack propagation within the gear component.

- ***Mesh conditions***

The 3D FE model is meshed with linear tetrahedral elements. The half-length and half-width of the contact area depend on the contact force applied by the rolling element. This necessitates a substantial mesh refinement in the vicinity of the rolling track to accurately define the Hertzian contact ellipse. To achieve this, a mesh size of 0.1 mm is employed. Additionally, a further mesh refinement constraint is implemented within a specific volume of interest, particularly where the crack is inserted. This refinement is crucial to obtain precise estimations of Stress Intensity Factors (SIFs), particularly when contact conditions are present.

- **Material behavior: Constitutive equations**

A fully elastic behavior of the steel gear and bearings was considered. Tensile tests on two steels representative of the case hardened layer and the core material in terms of carbon content did not reveal any significant effect of case hardening on the elastic properties.

- ***Boundary conditions***

The contact loads imposed by the bearings on the track were defined by functions based on Hertz pressures [20] corresponding to the local resultants of the forces imposed on each contact zone. Because rolling elements are not modeled, no friction is considered on the roller track.

To validate this procedure, the computed stress state was compared at various depths (0.2 mm and 1.0 mm) with that predicted by the Hertz theory. A good agreement was observed (error less than 5%).

- ***Residual stress modelling***

Case hardening (or nitriding) is applied on the gear to increase the hardness of its outer surface, and to induce biaxial compressive residual stresses that enhance its resistance to RCF. Depouhon and al. [21-24] proposed a multi-scale and multi-physical model of the nitriding process, based on the finite element method and an inverse method applied on measured residual stress profiles to introduce realistic residual stress field into a 3D finite element model. Considering a linear elastic behavior, the total strain (noted ε) is the sum of an elastic accommodation strain (noted ε_e), and an apparent volumetric eigenstrain (noted ε_F) reflecting all effects related to case-hardening (volume expansion, diffusion, precipitates) [24].

The present approach considers that the only consequence of case-hardening is the resulting apparent volumic eigenstrains ε_F. The elastic strain field ε_e is then generated to ensure the compatibility of the total strain ε, (Eq. (1)) [24]. Finally, residual stresses are deduced from Hooke's law.

$$\begin{cases} \text{Kinematic compatibility:} \\ \varepsilon = \varepsilon_e + \varepsilon_f \\ \varepsilon_f = \varepsilon_f \mathrm{I} \end{cases}$$

$$\begin{cases} \text{Equation of equilibrium:} \\ \mathrm{div}(\sigma) = 0 \end{cases} \quad (1)$$

$$\begin{cases} \text{Consitutive law:} \\ \quad \sigma = K\varepsilon_e \end{cases}$$

Because the eigenstrain ε_F is volumetric, numerical analogy with thermal diffusion problem was proposed. Consequently, to reproduce the residual stress profiles measured by X-ray diffraction on the gear, a thermal calculation first yields an equivalent temperature field, and the associated strains are deduced, using an equivalent thermal expansion coefficient.

Subsequently, using the elastic properties of the steel, which constitutes the gear, the residual stresses are prescribed and demonstrate a remarkable agreement with the experimental measurements. An initialization of the mechanical model is implemented, before the first loading increment, to introduce this residual stress field rough the equivalent thermal simulation.

- ***Cracks insertion and SIF estimation***

Finally, a crack representative of those observed in the part, was inserted in this model (Figure 2) using the adaptive meshing features available in the *Z-Cracks* software [25]. The crack was 20 mm long, 18 mm width, and inclined by 7° with respect to the contact surface. The straight crack front was thus positioned at a depth of 1.5 mm, which corresponds to the transition between the case-hardened layer and base material. The stress intensity factors were computed at the center-point of the crack front, using the G-θ method [26] in a discrete approach, as detailed by Vattré and Chiaruttini [27], assuming a frictionless contact between crack lips.

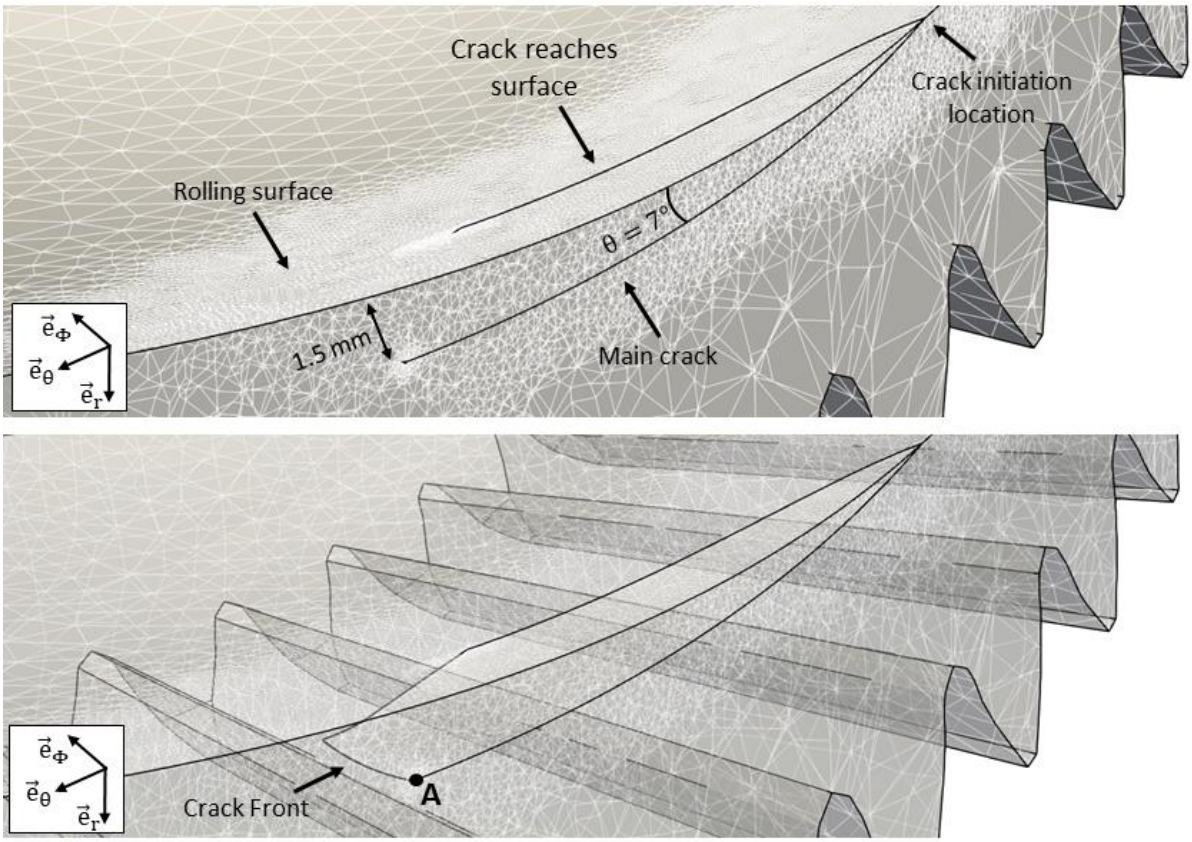

Figure 2 : Crack shape and position in the 3D FE model (Point A: center of the crack front)

RESULTS AND DISCUSSION

- ***Influence of the residual stress field***

A 3D FE computation was performed, using the previously presented model, considering only the carburization-induced residual stress field. The residual stress field induces a static K_{II} at the center of the crack front. Furthermore, Figure 3(a) shows that the crack in the case-hardened layer redistributes locally the residual stress.

Far from the crack (section line B), the stress state below the surface is biaxial compression until approximately 1.5mm in depth (figure 3(c)). However, just behind the crack front (section line A, figure 3(b)), due to the expansion imposed by the thermochemical process, a stress redistribution and a stress discontinuity between the crack flanks are observed: the upper flank is under tension, promoting the initiation of the secondary branches, while the lower flank is

under compression, inhibiting the initiation the microcracks.

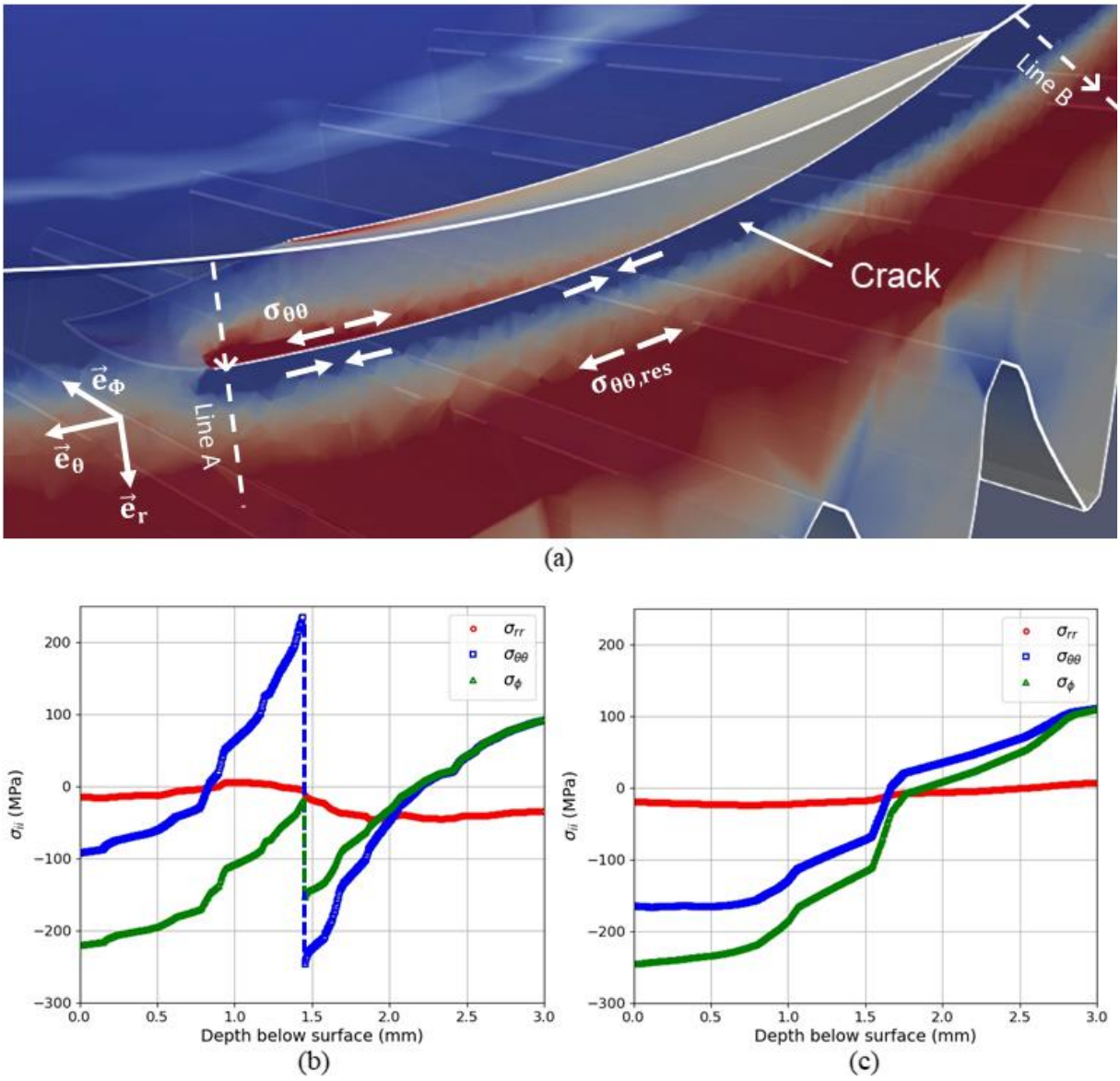

Figure 3 : (a) $\sigma_{\theta\theta}$ component of the residual stress field in the case-hardened layer with a crack, and evolution of the residual stress (b) close to the crack front (section line A), and (c) away from the crack front (section line B)

To highlight the influence of the residual stresses, figure 4 illustrates the opening or closure of a branch, normal to the main crack face, and positioned 0.1 mm behind the main crack front, on its upper (Figure 4(a)), or lower (Figure 4(b)) flank, when only the residual stresses are considered, and not the hertzian pressure due to RCF. The residual stresses tend to open the upper branch and to oppose the opening of the lower branch.

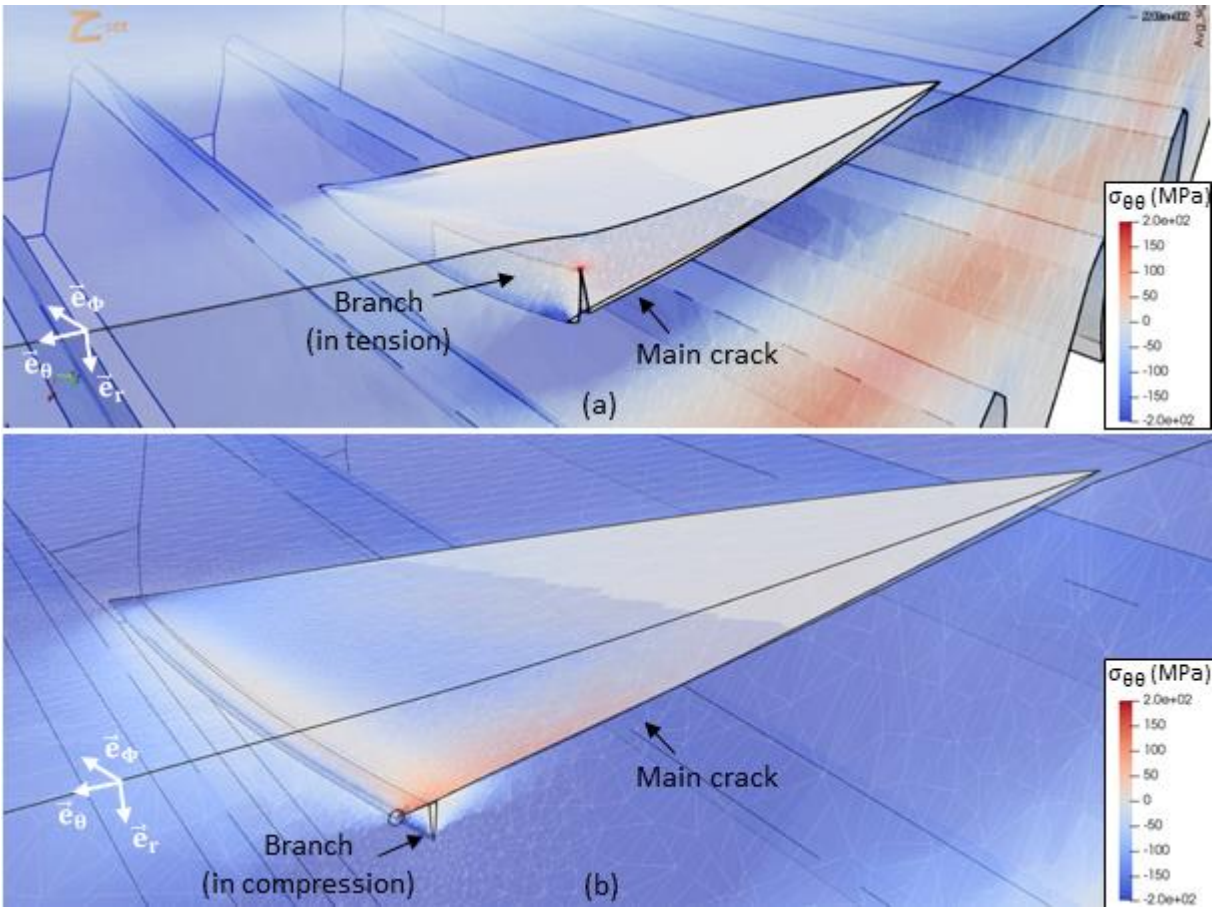

Figure 4 : Deformation of a branch initiated from a) the upper crack face or b) the lower crack face in the sliced 3D FE model subjected to the residual stress field only (deformation amplification x20).

- ***Loading cycle of a crack in RCF***

Figure 5 shows the evolution of the SIFs at the center of the main crack front (point A, Figure 3) during one passage of the bearing, plotted versus the projected distance on the surface between the considered point and the moving load. During hertzian loading, K_I decreases. As a result of an imprecise solution of the contact condition, fictitious negative K_I values are observed. This occurrence arises due to nodal interpenetration caused by the extremely high compressive normal stress in the vicinity of the singularity region. An asymmetric shear mode loading (R_{II} = -4.5) is observed, due to the static K_{II} imposed by the residual stresses, as mentioned above. At the center point A of the crack front, K_{III} is negligible. Figure 6 highlights the non-proportional mixed-mode loading of the crack in RCF, dominated by mode II, as

observed in the literature [1, 28, 29].

The computed ΔK_{II} is nearly ten times higher than ΔK_I, at least for frictionless contact. Even though crack face friction, enhanced by normal compression, should substantially reduce the effective ΔK_{II}, crack propagation in the case-hardened layer is probably driven by asymmetric cyclic mode II with a superimposed cyclic triaxial compression.

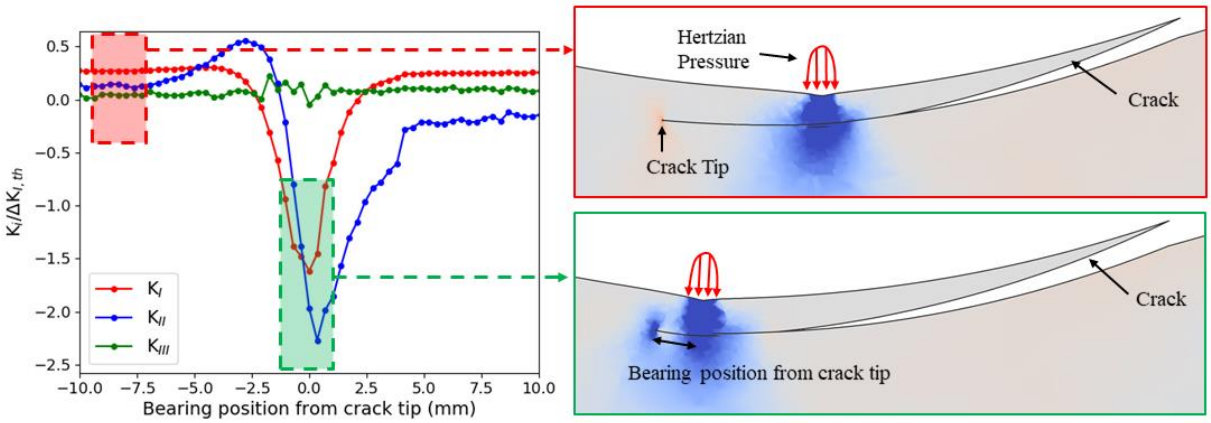

Figure 5 : K_I, K_{II} and K_{III} evolution during a RCF cycle with the residual stresses taken into account

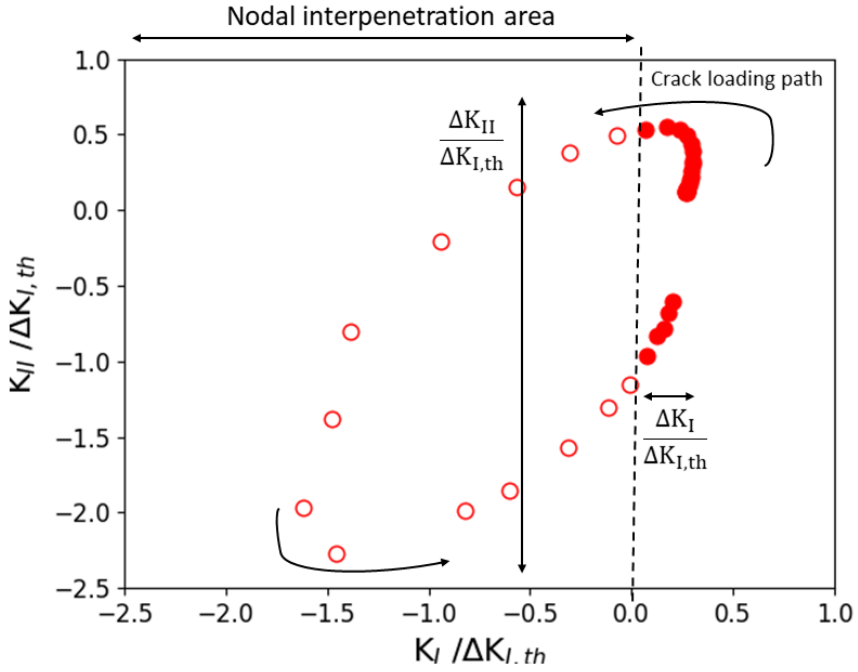

Figure 6 : K_I vs K_{II} evolution during a RCF cycle with the residual stresses taken into account

- ***Estimation of the branch orientation from the tip of the main crack***

To determine the orientation of potential branches, the angular evolution of the FICs for a branch at the main crack tip must be considered. Amestoy and Leblond [30, 31] proposed an expression of the stress intensity factors k_I^*, k_{II}^*, k_{III}* at the tip of an infinitesimal branch inclined by an angle θ, as a linear combination of the stress intensity factors K_I, K_{II}, K_{III} at the main crack tip, before branching:

$$\begin{pmatrix} {k_I}^* \\ {k_{II}}^* \\ {k_{III}}^* \end{pmatrix} = \begin{bmatrix} F_{I,I}(\theta) & F_{I,II}(\theta) & 0 \\ F_{II,I}(\theta) & F_{II,II}(\theta) & 0 \\ 0 & 0 & F_{III,III}(\theta) \end{bmatrix} \begin{pmatrix} K_I \\ K_{II} \\ K_{III} \end{pmatrix} (2)$$

Where the components $F_{I,I}(\theta)$, $F_{II,II}(\theta)$, $F_{III,III}(\theta)$, $F_{I,II}(\theta)$ et $F_{II,I}(\theta)$ depend on the bifurcation angle θ and have been tabulated by Amestoy and Leblond [30] in 2D, and by Leblond [32] in 3D.

Several calculations with the 3D FE model were performed considering the contact loads, for different main crack lengths, L_{main}: 3 mm, 7 mm, 14 mm and 20 mm, corresponding to various crack front depths (h_{main}) inside the case-hardened layer, assuming a frictionless contact along the main crack flanks. A rolling contact cycle was simulated, and the min and max values of ${k_I}^*(\theta)$ and ${k_{II}}^*(\theta)$ were calculated from the min and max values of K_I and K_{II}, using equation 2. The amplitudes $\Delta{k_I}^*(\theta)$ and $\Delta{k_{II}}^*(\theta)$ and the R ratio of the potential branch, ${R_I}^*(\theta) = \frac{{k_{I,min}}^*(\theta)}{{k_{I,max}}^*(\theta)}$ were deduced.

Figure 7 compares the angular evolution of $\Delta{k_I}^*(\theta)$ and $\Delta{k_{II}}^*(\theta)$ around the crack front with, and without, the consideration of residual stresses. The peaks values of $\Delta{k_I}^*(\theta)$ are found at ±76°, in good agreement with the initiation angle of the secondary branches observed in the part, which are around 75-80° (figure 1a).

However, for each main crack length studied, the residual stresses induce an asymmetry of the angular distribution of $\Delta k_I^*(\theta)$, favoring branching at $\theta = 76°$, that is: bifurcation towards the rolling surface (likely to induce spalling, if the branch reaches the surface), rather than bifurcation at -76°, towards the depth. The deeper the main crack grows through the case-hardened layer, the stronger the asymmetry of $\Delta k_I^*(\theta)$. This increase in $\Delta k_I^*(\theta)$ can be explained by the static negative K_{II} generated at the main crack front by the residual stresses.

L_{main} & h_{main}	Without residual stresses	With residual stresses
3 mm 0.37 mm	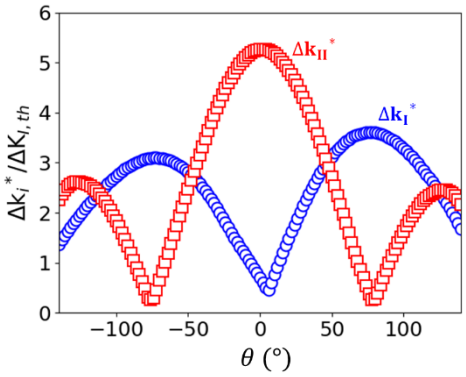 $\frac{\Delta K_I}{\Delta K_{I,th}} = 0.7, \frac{\Delta K_{II}}{\Delta K_{I,th}} = 5.3$	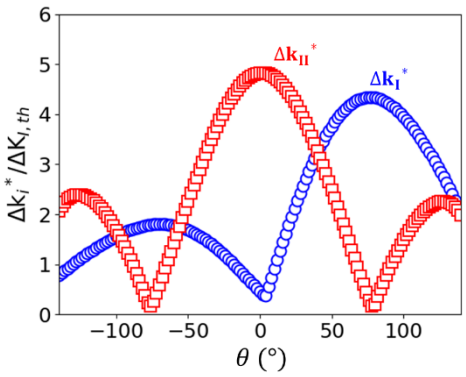 $\frac{\Delta K_I}{\Delta K_{I,th}} = 0.5, \frac{\Delta K_{II}}{\Delta K_{I,th}} = 4.8, \sigma_{res} = -210$ MPa

7 mm 0.64 mm	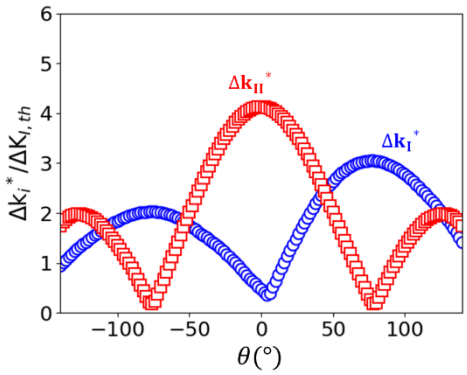 $\frac{\Delta K_I}{\Delta K_{I,th}} = 0.5, \frac{\Delta K_{II}}{\Delta K_{I,th}} = 4.1$	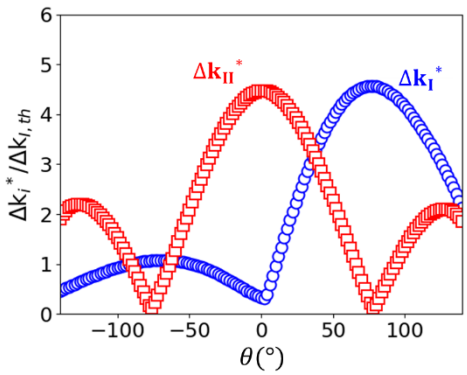 $\frac{\Delta K_I}{\Delta K_{I,th}} = 0.3, \frac{\Delta K_{II}}{\Delta K_{I,th}} = 4.5, \sigma_{res} = -210$ MPa
14 mm 1.28 mm	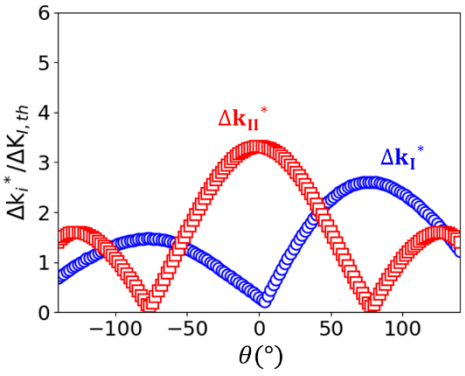 $\frac{\Delta K_I}{\Delta K_{I,th}} = 0.3, \frac{\Delta K_{II}}{\Delta K_{I,th}} = 3.3$	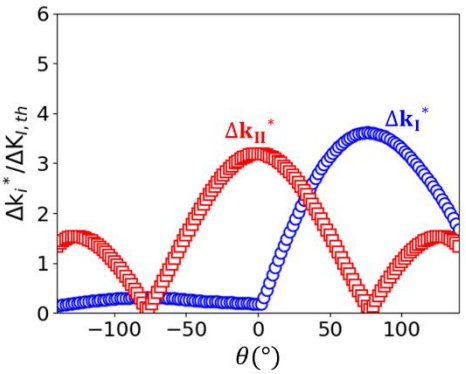 $\frac{\Delta K_I}{\Delta K_{I,th}} = 0.2, \frac{\Delta K_{II}}{\Delta K_{I,th}} = 3.2, \sigma_{res} = -130$ MPa
20 mm 1.55 mm	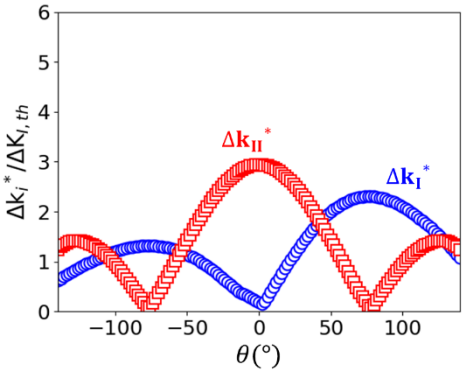 $\frac{\Delta K_I}{\Delta K_{I,th}} = 0.2, \frac{\Delta K_{II}}{\Delta K_{I,th}} = 2.9$	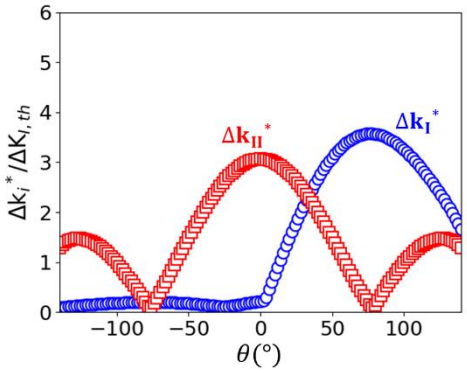 $\frac{\Delta K_I}{\Delta K_{I,th}} = 0.2, \frac{\Delta K_{II}}{\Delta K_{I,th}} = 3.1, \sigma_{res} = -70$ MPa

Figure 7 : Evolution of Δk_I^* (θ) and Δk_{II}^* (θ) for different main crack lengths during a RCF loading cycle. σ_{res} is

the residual stress normal to the branch crack, at its tip

Table 1 summarizes the evolution of R_I^* computed for the angular maxima of Δk_I^* of the branches growing towards the surface ($\theta = 76°$) or towards the depth ($\theta = -76°$).

The R_I^* ratio of the branches pointing towards the surface is increased by the residual stresses, making their propagation faster, while the R_I^* ratio of the branches pointing towards the depth is sharply reduced.

The thresholds for mode I fatigue crack growth in the steel, which constitutes the gear, and in a steel with a higher carbon content, representative of the case hardened layer were determined for various R ratios. The results are not reported here for confidentiality reasons. However, the comparison of $\Delta k_I^*(\theta)$ with the measured thresholds suggests that in the presence of residual stresses, the branches pointing towards the depth should not be able to propagate, as $\Delta k_I^*(-76°) \leq \Delta K_{I,th}$.

By contrast, the computed values of $\Delta k_I^*(76°)$ are much higher than the threshold, so that the branches pointing towards the surface might be able to propagate, once initiated. The purpose of the next paragraph is to determine whether or not they can reach the surface, depending on the depth of their initiation site.

Table 1 : Influence of the residual stresses on the R ratio of a branch for various main crack lengths

	Branch pointing towards the surface $R_I^*(+76°)$		Branch pointing towards the depth $R_I^*(-76°)$	
L_{main} (mm)	Without σ_{res}	With σ_{res}	Without σ_{res}	With σ_{res}
3	- 0.7	- 0.3	- 1.2	- 2.4

7	- 0.7	- 0.2	- 1.5	- 4.3
14	- 0.6	- 0.1	- 1.8	- 11.6
20	- 0.6	- 0.06	- 1.8	- 17.7

- ***Further propagation of branches pointing towards the surface.***

Once initiated, the branches pointing towards the surface can either propagate until they form spalls on the bearing race, or stop growing before reaching the surface, depending on the evolution of their loading.

The previous paragraph considered only the initiation of an incipient, infinitesimal branch crack from the main crack front. A branch crack with a finite length, s, inclined by 80° relative to the main crack growth direction, and positioned at a distance b behind its front was inserted in the 3D FE model (figure 8). In fatigue, the initiation of a branch does not necessarily stop the growth of the main crack in mode II, so that a branch, initiated from the tip can be left behind due to the main crack growth [18]. Such a branch, mostly loaded in mode I however has a shielding effect on the main crack, as illustrated below, by the computations of ΔK_I for the branch and ΔK_{II} for the main crack.

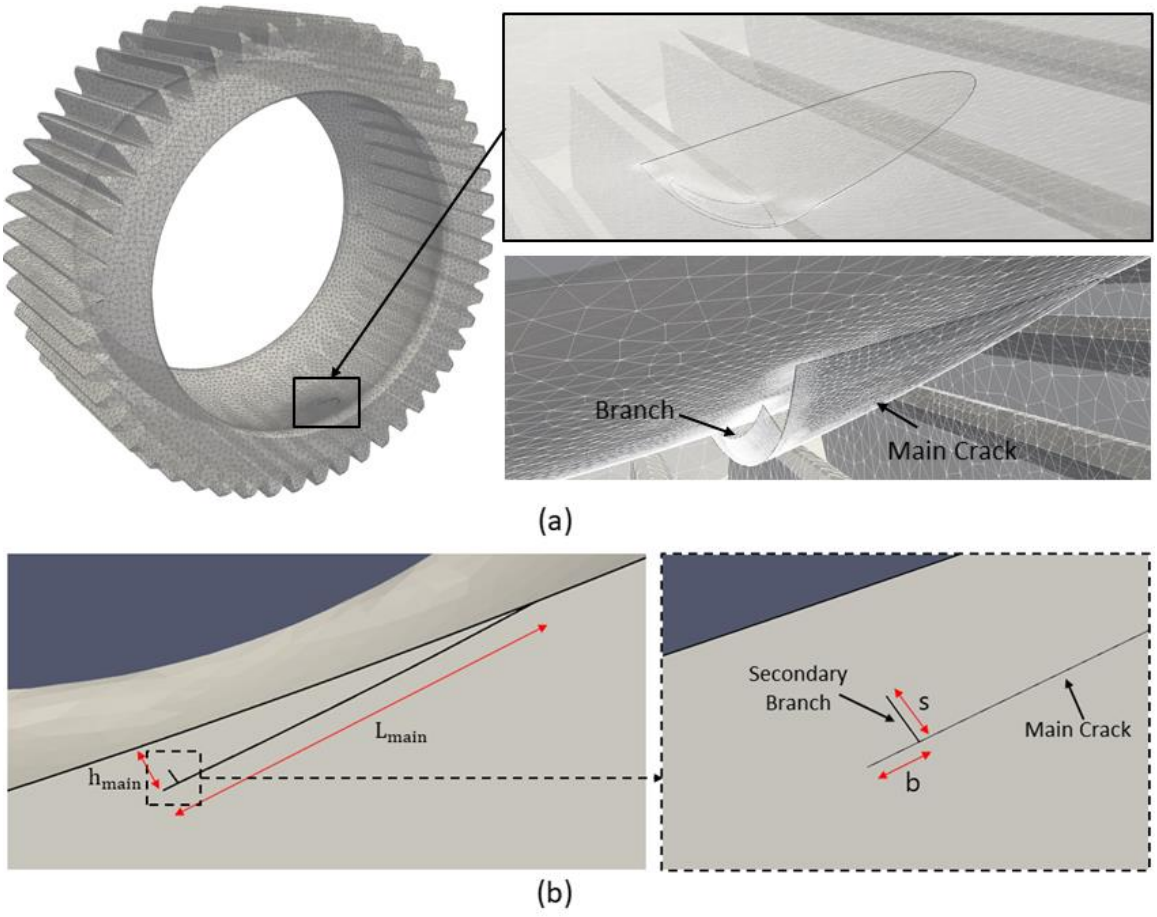

Figure 8 : Calculation configuration with a secondary branch inserted on the upper flank of the main crack in the 3D FE model

Two parametric studies were performed, considering both the contact loads, and the residual stresses, and assuming a frictionless contact between the lips of the main crack and of the branch.

- Study 1: the main crack length L_{main} was varied from 3 mm to 14 mm, while keeping the branch parameters constant: b = 0.1 mm and s = 0.1 mm.
- Study 2: the main crack length was fixed, at L_{main} = 7 mm, 10 mm or 14 mm, as well as the secondary branch distance to its front, b = 0.1mm, while the branch crack length was varied.

- ***Study 1: Influence of the branch initiation site depth in the case-hardened layer***

Figure 9 shows the evolutions with the depth of the main crack front, of ΔK_I at the branch crack

tip and ΔK_{II} at the center of the main crack front, with or without the presence of the branch.

ΔK_I at the branch crack tip is 5.7 times $\Delta K_{I,th}$ when the main front is 0.37 mm below the surface, and 4.1 times $\Delta K_{I,th}$ for a depth of 1.23 mm (figure 9). So, a 100 µm-long branch crack, initiated from a main crack in this depth range should grow further. Figure 9 also shows that the longer the main crack, the smaller ΔK_I at the branch crack tip, and the more difficult it becomes for this branch to reach the surface.

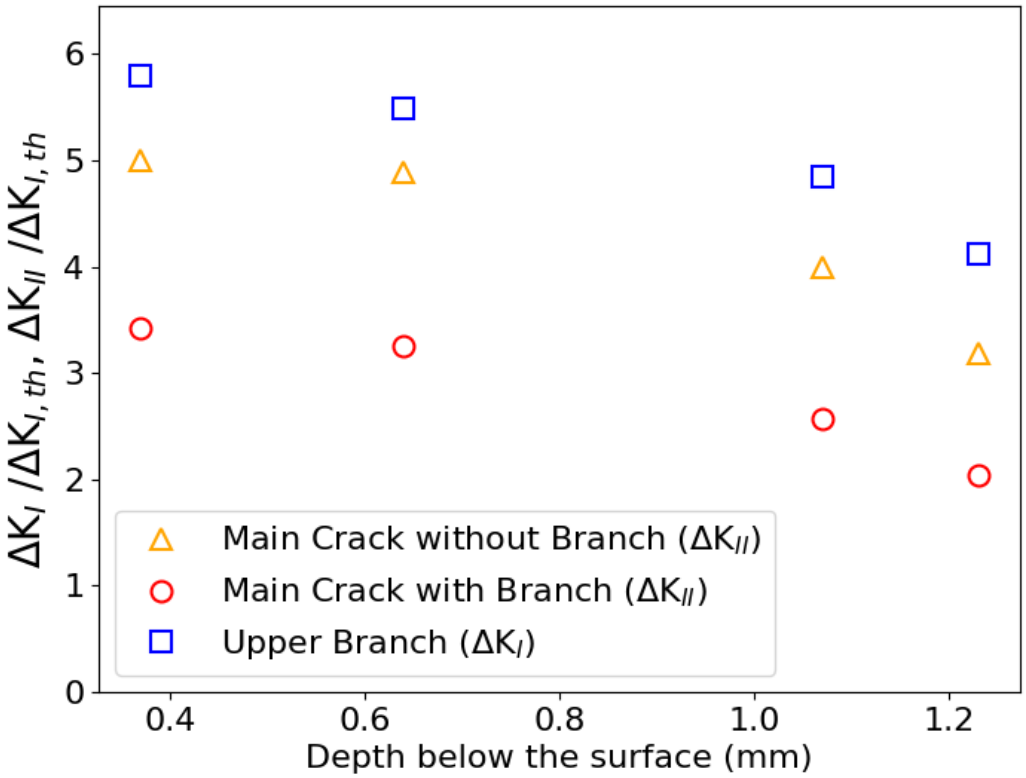

Figure 9 : Evolutions of the normalized ΔK_I at a stationary branch crack tip, and normalized ΔK_{II} at the main (propagating) crack tip, with or without the presence of a 0.1mm-long branch crack, inclined by 80° at 0.1mm from the tip, on the upper flank.

As expected, ΔK_{II} decreases when the crack front moves away from the contact surface. A significant shielding effect, -that is: a 30-35% reduction of the main crack driving force due to

the presence of the 100 µm-long branch crack- is observed. It will be shown below that the shielding effect increases with the branch crack length.

- ***Study 2: Evolution of the branch crack growth rate***

The purpose of this part is to explain why the branches seem, as suggested by figure 1a, to stop propagating at a certain depth below the raceway, thus limiting surface spalling.

The evolution of ΔK_I with the length s of a branch, initiated from a main crack with fixed length, L_{main}, will be studied.

Figure 10(a) shows the evolution of ΔK_I as a function of the depth at which the branch front is located for the three lengths L_{main} studied. For L_{main} = 7 mm ($\frac{\Delta K_{II}}{\Delta K_{I,th}} = 3.3$), initially, the branch crack tip is located at a depth of 0.54 mm in the case-hardened layer, ΔK_I is equal to 5.5 times $\Delta K_{I,th}$, but decreases slightly as the branch crack propagates, although still remaining well above $\Delta K_{I,th}$.

For L_{main} = 10 mm ($\frac{\Delta K_{II}}{\Delta K_{I,th}} = 2.6$) , the front of the branch crack is initially 0.97 mm deep, and ΔK_I is 4.8 times $\Delta K_{I,th}$. ΔK_I remains constant until the branch crack tip reaches 0.57 mm below the raceway, at which point ΔK_I begins to decrease. This branch crack stops growing before reaching the surface. The same observation is made for L_{main} = 14 mm ($\frac{\Delta K_{II}}{\Delta K_{I,th}} = 2.1$).

Thus, from an initiation depth between 0.54 mm and 0.97 mm, the branch cracks have no longer the capacity to generate surface spalling at a given nominal threshold depth. Moreover, the calculations were performed with a frictionless sliding contact, and assuming the main crack to be stationary. Taking into account crack face friction and the propagation of the main crack would further decrease ΔK_I at the branch crack tip, leading to an even earlier arrest at a threshold

depth closer to the value of 0.35 mm depth observed in figure 1. Figure 10(b) shows that, considering the residual stresses or not, the branch crack should stop propagating within the carburized layer, for L_{main} = 14 mm, while it would be able to continue to grow towards the surface, for L_{main} = 7 mm.

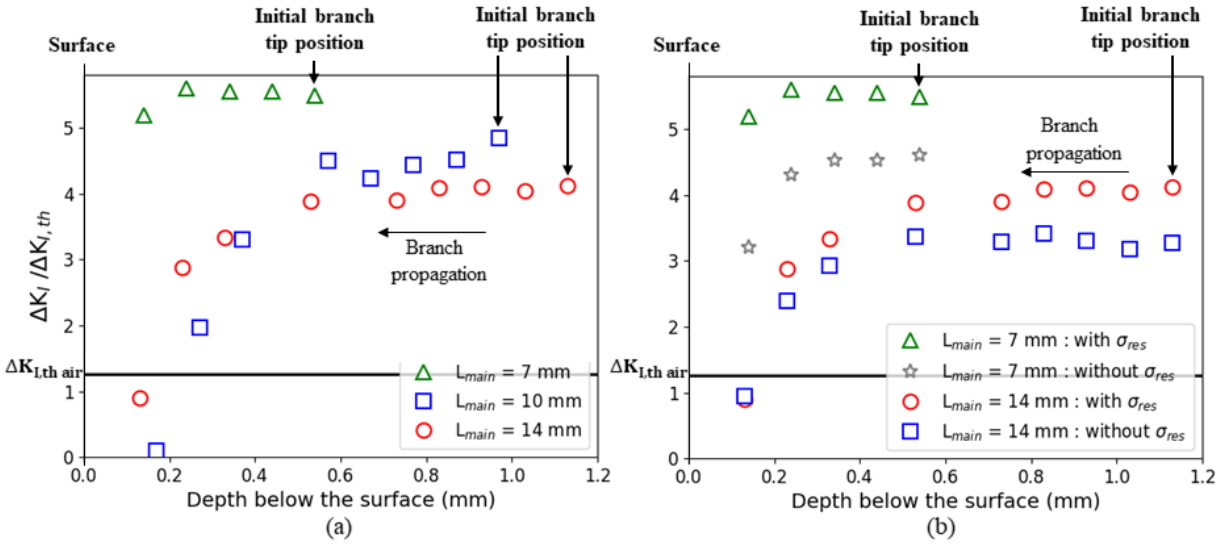

Figure 10 : (a) ΔK_I evolution for branches pointing towards the surface, as a function of the depth of their front in the case-hardened layer, and (b) Influence of residual stresses on branch arrest (L_{main} = 7 mm and L_{main} = 14 mm)

Figure 11 illustrates, for L_{main} = 7, 10 and 14 mm, the evolution of the branch-crack-induced reduction of ΔK_{II} at the center of the (stationary) main crack front, as the branch crack propagates towards the surface. The normalized ΔK_{II} is plotted as a function of the ratio s/b (with s, the branch crack length, and b, the (fixed) distance of its initiation point from the main crack tip, see Figure 8(b)). In each case, the shielding effect increases significantly with the branch crack length, but tends to saturate, whatever L_{main}, when the s/b ratio (initially equal to 1) reaches approximately 2.

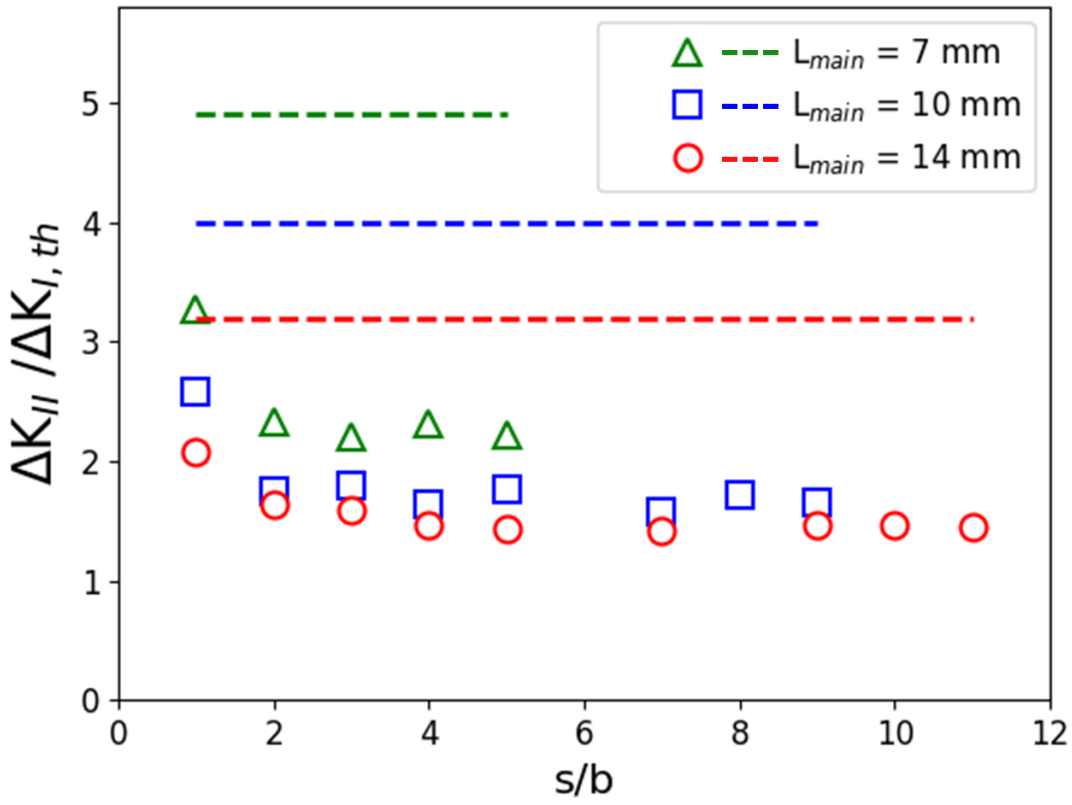

Figure 11: Evolution of the normalized ΔK_{II} at the (stationary) main crack tip, as the branch crack (of length s, initiated at a distance b from the main crack tip) grows. The dotted lines represent, for each main crack length considered, the normalized ΔK_{II} without any branch. The difference between symbols and dotter line is whether, or not, branch crack is considered.

CONCLUSIONS AND FURTHER COMMENTS

A 3D numerical study of the initiation and growth of secondary branches in the case-hardened layer of a helicopter gear was performed, to explain some experimental observations. It showed that:

- Case-hardening-induced residual stresses generate :
    - A tensile stress field on the upper side of the main crack, favoring the initiation of branches;
    - A compressive field on the lower side of the main crack, preventing potential

branches from initiating.

- The observed branch initiation angle of about 75° - 80° corresponds to the direction where Δk_I^* is maximum.
- In the presence of residual stresses, the R_I^* ratio of the branches remains above -0.3 for the surface-pointing branches, while it is below -2.4 for the inward-pointing branches, making the propagation of the latter more difficult.
- The surface-pointing branches have a significant shielding effect: 30-35% reduction in $\Delta K_{II,nom}$ at the main crack tip, when the ratio s/b is equal to 1 (where b stands for the distance between the branch crack initiation point and the main crack tip). This shielding effect rises the branch crack length, s, but tends to saturate, when $s/b \approx 2$.
- While the branches initiated when the main crack is still shallow can easily reach the surface, and generate surface spalling, this is no more the case for branches initiated when the main crack is deeper.

From a broader damage detection point of view, this study highlights 2 main stages in the damage evolution:

- The first stage corresponds to a direct correlation between the growth rate of a main crack towards the depth of the piece, and the growth towards the contact surface of subsurface-initiated branch cracks, whose emergence is responsible for the release of metal particles. It occurs in the early stage of the main crack propagation, at a shallow depth (in this study, less than 0.54 mm). The computations have shown that it is very improbable that surface-initiated cracks in RCF never release any metal particle.
- On the contrary, the second stage corresponds to a decoupling between the main crack growth, in mode II, beyond a certain depth (0.54 mm in this study) and surface spalling. In this stage, if spalling continues, it cannot be due anymore to the continued inwards

growth of the same “main crack”, but must rather be triggered by the initiation of new such cracks from the contact surface, which is already damaged by spalling.

REFERENCES

[1] Sadeghi F, Jalalahmadi B, Slack TS, Raje N, Arakere NK. A review of rolling contact fatigue. J Tribol., 2009;131:041403. https://doi.org/10.1115/1.3209132.

[2] Ren Z, Li B, Zhou Q. Rolling contact fatigue crack propagation on contact surface and subsurface in mixed mode I+II+III. Wear, 2022;506-507:204459. https://doi.org/10.1016/j.wear.2022.204459

[3] Kunzelmann B, Rycerz P, Xu Y, Arakere NK, Kadiric A. Prediction of rolling contact fatigue crack propagation in bearing steels using experimental crack growth data and linear elastic fracture mechanics. International Journal of Fatigue, 2023;168:107449. https://doi.org/10.1016/j.ijfatigue.2022.107449

[4] Coelho L, Batista AC, Nobre JP, Marques MJ. Rolling and Rolling-Sliding Contact Fatigue Failure Mechanisms in 32 CrMoV 13 Nitrided Steel – An Experimental Study. Appl. Sci., 2021; 11:10499. : https://doi.org/10.3390/app112110499

[5] Bower AF. The Influence of Crack Face Friction and Trapped Fluid on Surface Initiated Rolling Contact Fatigue Cracks. ASME J. Tribol., 1988; 110:704–711.

[6] Nelias, D, Dumont ML, Champiot, F, Vincent A, Girodin, D, Fougeres, R, and Flamand, L. Role of Inclusions, Surface Roughness and Operating Conditions on Rolling Contact Fatigue. ASME J. Tribol., 1999; 1212:240–251

[7] Keer LM, Bryant MD. A pitting model for rolling contact fatigue. J Lubr Technol, 1983; 105:198–205. https://doi.org/10.1115/1.3254565.

[8] Lou B, Han L, Lu Z, Liu S, and Shen F. The Rolling Contact Fatigue Behaviors in

Carburized and Hardened Steel. Fatigue 90: Proceedings of the Fourth International Conference on Fatigue and Fatigue Thresholds, Honolulu, HI, H. Kitagawa and T. Tanaka, eds., 1990: 627–632.

[9] Rycerz P, Olver A, Kadiric A. Propagation of surface initiated rolling contact fatigue cracks in bearing steel. International Journal of Fatigue 2017; 97:29–38. https://doi.org/10.1016/j.ijfatigue.2016.12.004.

[10] Suresh S. Fatigue crack deflection and fracture surface contact: Micromechanical models. Metallurgical Transactions A, 1985;16(1):249–260. doi:10.1007/BF02815306.

[11] Jessop C, Ahlström J, Hammar L, Fæster S, Danielsen HK. 3D characterization of rolling contact fatigue crack networks. Wear, 2016; *366-367:*392–400. https://doi.org/10.1016/j.wear.2016.06.027

[12] Dubourg MC, Lamacq V. A Predictive Rolling Contact Fatigue Crack Growth Model: Onset of Branching, Direction, and Growth—Role of Dry and Lubricated Conditions on Crack Patterns. Journal of Tribology, 2002; 124:680–8. https://doi.org/10.1115/1.1479698.

[13] Wong SL, Bold PE, Brown MW, Allen RJ. Fatigue crack growth rates under sequential mixed-mode I and II loading cycles. Fatigue Fract Eng Mater Struct, Aug. 2000;23(8):667–74.

[14] Otsuka A, Sugawara H, Shomura M. A test method for Mode II fatigue crack growth relating to a model for rolling contact fatigue. Fat Frac Eng Mat Struct., 1996;19 (10):1265–75. https://doi.org/10.1111/j.1460-2695.1996.tb00949.x.

[15] Otsuka A, Fujii Y, Maeda K, Ogawa T. Mode II fatigue crack growth as influenced by a compressive stress applied parallel to the crack path. Fatigue Crack Path 2003.

[16] Zaid M, Bonnand V, Doquet V, Chiaruttini C, Pacou D, Depouhon P. Fatigue crack growth in bearing steel under cyclic mode II + static biaxial compression. International Journal of

Fatigue, 2022; 163:107074. https://doi.org/10.1016/j.ijfatigue.2022.107074

[17] Kfouri AP. A crack in a linear-elastic material under mode II loading, revisited. Fat Frac Eng Mat Struct., 1999; 22:445–8. https://doi.org/10.1046/j.1460-2695.1999.00178.x.

[18] Doquet V, Frelat J. Branch crack development from the flank of a fatigue crack propagating in mode II: Propagation of fatigue cracks in mode II. Fatigue & Fracture of Engineering Materials & Structures, 2001; 24:207–14. https://doi.org/10.1046/j.1460-2695.2001.00384.x.

[19] Nishizawa H, Ogawa T. Mode II fatigue crack growth characteristics and experimental evaluation of the crack driving force. Journal of the Society of Materials Science 2005, 54(12):1295-1300.

[20] Hertz H. Ueber die Berührung fester elastischer Körper. Journal für die reine und angewandte Mathematik (Crelles Journal), 1882; 92:156–171. doi:10.1515/crll.1882.92.156.

[21] Depouhon P, Sprauel JM, Mailhé M, Mermoz E. Modeling of distorsions induced by the nitriding process. Mechanics & Industry, 2015; 16:107.

[22] Depouhon P, Sprauel JM, Mailhé M, Mermoz E. Mathematical modeling of residual stresses and distortions induced by gas nitriding of 32CrMoV13 steel. Computational Materials Science, 2014; 82:178-190.

[23] Depouhon P, Sprauel JM, Mermoz E. Prediction of residual stresses and distortions induced by nitriding of complex 3D industrial parts. CIRP Annals, 2015; 64(1):553-556.

[24] Lemaitre J, Chaboche J-L. Mechanics of Solid Materials. 1st ed. Cambridge University Press; 1990. https://doi.org/10.1017/CBO9781139167970.

[25] Chiaruttini V, Riolo V, Feyel F. Advanced remeshing techniques for complex 3D crack propagation. vol. 1, Beijing: 2013, 547–55.

[26] Destuynder, Ph., Djaoua, M. and Lescure, S. Quelques remarques sur la mécanique de la

rupture élastique. *Journ. Mécanique Théorique & Appliquée* 1983 ; 2: 113–135

[27] Vattré A, Chiaruttini V. Singularity-free theory and adaptive finite element computations of arbitrarily-shaped dislocation loop dynamics in 3D heterogeneous material structures, Journal of the Mechanics and Physics of Solids, 2022;167:104954. https://doi.org/10.1016/j.jmps.2022.104954

[28] Kapoor A, Moreales Espejel GE, Olver AV. A shakedown analysis of simple spur gears, Tribology Transactions, 2002; 45:103-109.

[29] Canadinc D, Sehitoglu H, Verzal K. Analysis of surface crack growth under rolling contact fatigue. International Journal of Fatigue, 2008; 30:1678-1689.

[30] Amestoy M, Leblond JB. Crack paths in plane situations—II. Detailed form of the expansion of the stress intensity factors. International Journal of Solids and Structures, 1992;29(4):465–501. doi:10.1016/0020-7683(92)90210-K.

[31] Amestoy M, Bui HD, Van KD. Déviation infinitésimale d'une fissure dans une direction arbitraire. Comptes Rendus Acad Sciences de Paris 1979:99–102.

[32] Leblond JB. Crack paths in three-dimensional elastic solids. i: two-term expansion of the stress intensity factors—application to crack path stability in hydraulic fracturing. International Journal of Solids and Structures, 1999;36(1):79–103. doi:10.1016/S0020-7683(97)00276-X.